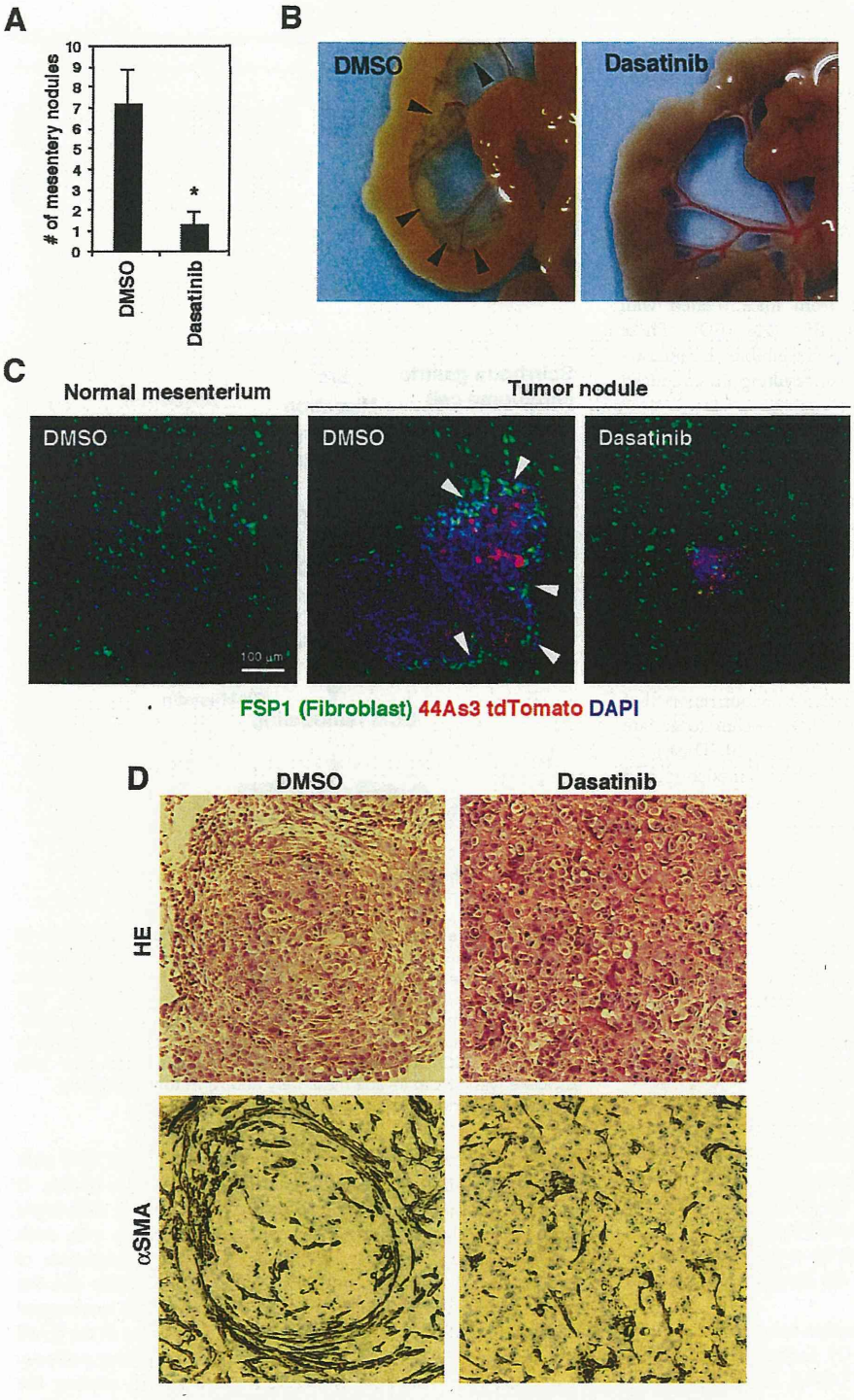

Figure 6. Dasatinib suppresses peritoneal dissemination of SGC cells and their association with stromal fibroblasts in vivo. A, 44As3 cells were intraperitoneally injected into nude mice and DMSO or dasatinib was administered via intraperitoneal injection. The number of mesentery nodules was calculated as described in the Materials and Methods. Bars show mean ± SEM ($n=10$). *, $p<0.005$ by Mann-Whitney test. B, Representative macroscopic views of metastatic tumor nodules (arrowheads) formed in the mesentery. C, Immunofluorescence analysis of the mouse mesenteries bearing tdTomato-labeled 44As3 tumor nodules. Arrowheads denote the regions where FSP1 positive stromal fibroblasts were accumulated around tumor nodules. D, Mesentery nodules were stained with hematoxylin and eosin and anti-αSMA antibody for histological examination.

doi:10.1371/journal.pone.0085485.g006

Table 1. Effect of dasatinib on peritoneal dissemination of 44As3 cells.

Treatment	Ascites	Metastasis				
		Omentum	Mesentery	Parietal Peritoneum	Diaphragm	Liver
DMSO	5/10	10/10	10/10	5/10	5/10	2/10
Dasatinib	0/10	1/10	4/10	0/10	2/10	0/10

Number of mice bearing ascites or tumor at the indicated site per total number of mice.
doi:10.1371/journal.pone.0085485.t001

SFs positive for αSMA, while those from mice treated with dasatinib contained significantly less SFs (Fig. 6D). These observations suggest that dasatinib treatment inhibits the interaction between SGC cells and SFs in vivo, resulting in a reduced peritoneal dissemination of SGC cells.

Discussion

In spite of their highly invasive behavior in vivo, we observed that SGC cells alone had a low invasive ability by themselves on both 3D Matrigel and 2D gelatin matrix. In contrast, SFs had some invasive and ECM remodeling activities that were markedly promoted by coculture with SGC cells. We discovered that SGC cells and SFs form invasive foci in which SFs constitute the core invading structures. In addition, SGC cells were physically attached to SFs in these structures and co-invaded the 3D Matrigel. These results are consistent with a previous report that SFs generate tracks in ECM by mechanical remodeling to initiate and lead invasion of squamous cell carcinoma cells [6]. Therefore, SFs potentially play an essential role in ECM remodeling and mediate invasion of SGC cells (Fig. 7). The increased proliferation of fibroblasts observed within SGC lesions may thus contribute to the rapid infiltration of SGC cells.

Mounting evidence suggests that stromal ECM composition and alterations in its structure foster tumor progression [24]. This process seems to largely depend on secretion, mechanical remodeling, and crosslinking of ECM components by SFs. Considering that the pathological features of SGC include severe fibrosis and resulting stiffening of the gastric wall, these changes in the biophysical properties of the tumor stroma may promote the invasion of SGC cells. Furthermore, SGC sometimes causes massive contractions of the stomach wall in the disease progression. Our results have shown that SGC cells enhance actomyosin-mediated contractility of SFs, resulting in mechanical remodeling and contraction of the ECM. Therefore, SF contraction stimulated by SGC cells may serve multiple roles in the pathogenesis of SGC, such as hardening and contraction of the gastric wall. Since the matrix rigidity is known to support invasiveness of cancer cells [25], enhancement of rigidity of tumors by cooperation between SGC cells and SFs might contribute the invasive properties of SGC.

It has been established that the interaction between cancer cells and SFs is mediated by soluble factors [1]. Indeed, several studies showed that soluble factors, including TGF-β, HGF, and bFGF, mediate stimulation of myofibroblasts phenotypes of SFs by SGC cells [15,26], as well as enhancement of the growth and invasive phenotypes of SGC cells by SFs [13,15,27–30]. To the contrary, Semba et al. reported that direct interaction, but not soluble factors, of SGC cells and SFs increases SF proliferation and invasive properties of SGC cells [14]. Consistent with this result, in our experiments conditioned medium from SGC cells could not recapitulate the phenotypes observed in the coculture experiments.

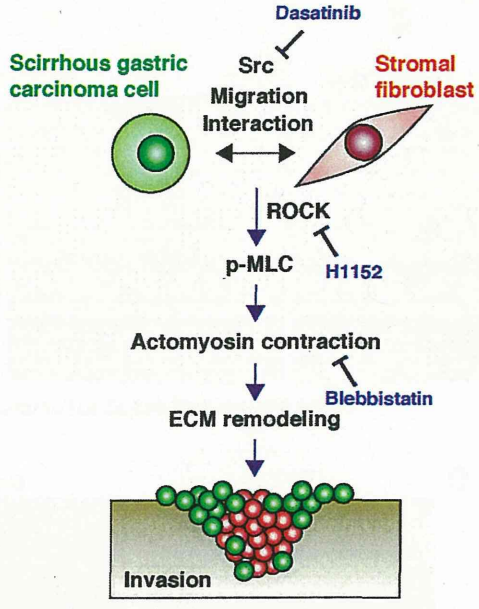

Figure 7. Schematic diagram of the SF-mediated invasion of SGC cells. SGC cells and SFs physically interact with each other through active migration and cell-cell contact, which is dependent on Src activity and therefore blocked by dasatinib treatment. This interaction promotes Rock-dependent phosphorylation of MLC, resulting in actomyosin contraction and mechanical ECM remodeling during invasion of SGC. In peritoneal dissemination, SGC cells may also associate with SFs to invade mesentery and form tumor nodules.
doi:10.1371/journal.pone.0085485.g007

These results indicate that a direct association between SGC cells and SFs, in addition to communication via soluble factors, is required for their full biological interactions. Indeed, time-lapse imaging revealed that the 2 cell types communicate with each other by strong physical associations during the formation of invasive foci. Moreover, coculturing SGC cells and SFs did not affect the myofibroblast phenotype as revealed by the unchanged expression of αSMA. Consequently, direct interaction of the 2 cell types leads to the activation of an intracellular signaling pathway that regulates actomyosin contractility, rather than altering the myofibroblast phenotype. We found that Rock is a critical regulator of the formation of invasive foci. Therefore, Rock/MLC signaling seems to play an essential role in mediating ECM remodeling and invasion by SGC and SFs. Next challenge will be to identify molecules directly involved in the physical interaction between SGC cells and SFs. Because VCAM-1 and integrin α4 were previously identified as potential mediators of their direct interaction [14], these molecules may also play a role in the

formation of invasive foci and invasive growth and dissemination of SGC.

We observed that Src inhibition by dasatinib significantly blocked the formation of invasive foci in 3D culture by impairing cell migration and resulting physical cell associations (Fig. 7). However, it did not affect mechanical gelatin remodeling by SGC cells and SFs in 2D culture. Because the two cell types were intermingled and in close proximity to each other in 2D culture condition, they may not require Src activity to physically interact. Nevertheless, this idea does not rule out the possibility that Src has distinct functions in SF-mediated invasion. Calvo et al. recently reported that mechanical remodeling and stiffening of ECM by CAFs induces YAP activation via Src-mediated mechanotransduction, which in turn promotes expression of cytoskeletal proteins and contractile phenotypes of CAFs, thus establishing a positive feedback loop [31]. At least in our experimental system, acute effect of dasatinib seems to be the inhibition of the interaction between SGC cells and SFs as described above. However, it is possible that long-term treatment of dasatinib, like in SGC xenograft study in vivo, affects contractile phenotypes of SFs due to decreased transcriptional activity of YAP. Therefore, it will be interesting to explore the role of YAP-dependent matrix stiffening by CAFs in invasive progression and peritoneal dissemination of SGC.

The formation of invasive foci was preferentially observed in SGC cell lines among gastric cancer cell lines, suggesting that this was representative of some of the biological characteristics of SGC cells. Additionally, we demonstrated that invasion of SGC cells occurred only when they formed invasive foci with SFs. Therefore, analysis of the formation of invasive foci may be useful for the evaluation and quantification of SF-mediated invasion and the ECM remodeling activity of SGC cells. Indeed, we utilized this assay system to screen inhibitor library and identified dasatinib as a potent inhibitor of the interaction between SGC cells and SFs. Moreover, we demonstrated for the first time that dasatinib blocks accumulation of SFs around and within mesentery tumor nodules and effectively reduces peritoneal dissemination of SGC cells in mice. Peritoneal dissemination of SGC is associated with strong fibrosis at the metastasis sites and is a critical and poor prognostic factor [10]. Therefore, SFs may also support invasion of SGC cells into mesentery stroma and resulting formation of metastasis. Taken together, this experimental system may enhance the study of the biological interactions between SGC cells and SFs, allowing the identification of regulating compounds, and thus facilitate the development of new therapeutics for SGC.

Supporting Information

Figure S1 Characterization of the formation of invasive foci. A, Invasion depth of invasive foci formed by 44As3 and CaF37 cells on 3D Matrigel. Bars show mean ± SD (n = 20). *, $p<0.0001$ by Student's t-test. B, CaF37 cells were cultured either with 44As3 cells or conditioned medium (CM) of 44As3 cells on 3D Matrigel for 2 days. 44As3 cells were also cultured with conditioned medium of CaF37 cells. C, A representative scanned image of invasive foci formed by 44As3 and CaF37 cells on 3D Matrigel. D, The number of invasive foci was quantified and shown as the relative values. Bars show mean ± SEM ($n = 4$). *, $p<0.0005$; **, $p<0.000001$ by Student's t-test.
(TIF)

Figure S2 Cocultured 44As3 and CaF38 cells form invasive foci on 3D Matrigel and remodel gelatin matrix. A, Invasive foci formed by 44As3 and CaF38 cells. B, Relative number of invasive foci. Bars show mean ± SEM ($n = 4$). *, $p<0.01$ by Student's t-test. C, Gelatin remodeling activity of 44As3 and CaF38 cells. D, The areas of gelatin detachment were quantified and shown as relative values. Bars show mean ± SEM ($n = 5$). *, $p<0.001$ by Student's t-test.
(TIF)

Figure S3 Formation of invasive foci and remodeling of ECM by 44As3 and CaF37 cells were not blocked by GM6001. A, Gelatin remodeling activity of 44As3 and CaF37 cells in the absence or presence of GM6001 (10 μM). B, The areas of gelatin disruption. Bars show mean ± SEM ($n = 4$). C, MDA-MB-231 cells were cultured on fluorescent gelatin-coated cover slips in the absence or presence of GM6001 (10 μM) for 7 h. D, Formation of invasive foci by 44As3 and CaF37 cells in the absence or presence of GM6001 (10 μM). E, The relative number of invasive foci. Bars show mean ± SEM ($ns = 4$).
(TIF)

Figure S4 Representative images for inhibitor library screening. CellTracker-labeled 44As3 and CaF37 cells were cultured on 3D Matrigel in the absence or presence of indicated inhibitors (10 μM) for 2 days and observed by confocal microscopy.
(TIF)

Figure S5 Effect of PP2 and imatinib on the formation of invasive foci and gelatin remodeling by cocultured 44As3 and CaF37 cells. A, The effect of PP2 (10 μM) and imatinib (10 μM) on invasive foci formation by 44As3 and CaF37 cells. B, The relative number of invasive foci. Bars show mean ± SEM ($n = 5$ for PP2 and 3 for imatinib). *, $p<0.00005$ by Student's t-test. C, The effect of PP2 (10 μM) and imatinib (10 μM) on gelatin remodeling activity of 44As3 and CaF37 cells. D, The areas of gelatin disruption. Bars show mean ± SEM ($n = 3$).
(TIF)

Video S1 Formation of invasive foci by 44As3 and CaF37 cells. 44As3 and CaF37 cells were labeled with CellTracker Green and Red, respectively, and plated onto 3D Matrigel. The cells were imaged every 5 min by time-lapse fluorescence microscopy for 16 h. Play rate, 15 frames/sec. Still images are shown in Figure 2A.
(MOV)

Video S2 Remodeling of Matrigel by 44As3 cells. 44As3 cells were cultured on 3D Matrigel containing fluorescent microbeads. The cells and microbeads were imaged every 5 min by time-lapse fluorescence microscopy for 8 h 45 min. Play rate, 15 frames/sec.
(MOV)

Video S3 Remodeling of Matrigel by CaF37 cells. CellTracker Green-labeled CaF37 cells were cultured and imaged as in Video S2.
(MOV)

Video S4 Remodeling of Matrigel by 44As3 and CaF37 cells. 44As3 cells and CellTracker Green-labeled CaF37 cells were cocultured and imaged as in Video S2.
(MOV)

Video S5 Formation of invasive foci in the presence of DMSO (control). CellTracker Green-labeled 44As3 cells and CellTracker Orange-labeled CaF37 cells were cocultured on 3D Matrigel in the presence of DMSO. The cells were imaged every 5 min for 14 h 45 min. Play rate, 15 frames/sec.
(MOV)

Video S6 H1152 impairs formation of invasive foci. Cells were cultured and imaged as in Video S5 in the presence of H1152 (10 μM).
(MOV)

Video S7 Dasatinib impairs formation of invasive foci. Cells were cultured and imaged as in Video S5 in the presence of dasatinib (10 μM).
(MOV)

Table S1 List of inhibitors screened and their effects on the formation of invasive foci. The relative number of invasive foci and cytotoxicity against 44As3 and CaF37 cells are shown for each compound in the screen at 10 μM. Dasatinib and H1152 are highlighted in red.
(DOCX)

References

1. Calvo F, Sahai E (2011) Cell communication networks in cancer invasion. Curr Opin Cell Biol 23: 621–629.
2. Joyce JA, Pollard JW (2009) Microenvironmental regulation of metastasis. Nat Rev Cancer 9: 239–252.
3. Kalluri R, Zeisberg M (2006) Fibroblasts in cancer. Nat Rev Cancer 6: 392–401.
4. Bhowmick NA, Neilson EG, Moses HL (2004) Stromal fibroblasts in cancer initiation and progression. Nature 432: 332–337.
5. De Wever O, Demetter P, Mareel M, Bracke M (2008) Stromal myofibroblasts are drivers of invasive cancer growth. Int J Cancer 123: 2229–2238.
6. Gaggioli C, Hooper S, Hidalgo-Carcedo C, Grosse R, Marshall JF, et al. (2007) Fibroblast-led collective invasion of carcinoma cells with differing roles for RhoGTPases in leading and following cells. Nat Cell Biol 9: 1392–1400.
7. Goetz JG, Minguet S, Navarro-Lerida I, Lazcano JJ, Samaniego R, et al. (2011) Biomechanical remodeling of the microenvironment by stromal caveolin-1 favors tumor invasion and metastasis. Cell 146: 148–163.
8. Ikeguchi M, Miyake T, Matsunaga T, Yamamoto M, Fukumoto Y, et al. (2009) Recent results of therapy for scirrhous gastric cancer. Surg Today 39: 290–294.
9. Japanese Gastric Cancer A (1998) Japanese Classification of Gastric Carcinoma - 2nd English Edition. Gastric Cancer 1: 10–24.
10. Yashiro M, Hirakawa K (2010) Cancer-stromal interactions in scirrhous gastric carcinoma. Cancer Microenviron 3: 127–135.
11. Zhi K, Shen X, Zhang H, Bi J (2010) Cancer-associated fibroblasts are positively correlated with metastatic potential of human gastric cancers. J Exp Clin Cancer Res 29: 66.
12. Yashiro M, Chung YS, Nishimura S, Inoue T, Sowa M (1996) Peritoneal metastatic model for human scirrhous gastric carcinoma in nude mice. Clin Exp Metastasis 14: 43–54.
13. Fuyuhiro Y, Yashiro M, Noda S, Matsuoka J, Hasegawa T, et al. (2012) Cancer-associated orthotopic myofibroblasts stimulates the motility of gastric carcinoma cells. Cancer Sci 103: 797–805.
14. Semba S, Kodama Y, Ohnuma K, Mizuuchi E, Masuda R, et al. (2009) Direct cancer-stromal interaction increases fibroblast proliferation and enhances invasive properties of scirrhous-type gastric carcinoma cells. Br J Cancer 101: 1365–1373.
15. Fuyuhiro Y, Yashiro M, Noda S, Kashiwagi S, Matsuoka J, et al. (2011) Upregulation of cancer-associated myofibroblasts by TGF-beta from scirrhous gastric carcinoma cells. Br J Cancer 105: 996–1001.
16. Yanagihara K, Takigahira M, Tanaka H, Komatsu T, Fukumoto H, et al. (2005) Development and biological analysis of peritoneal metastasis mouse models for human scirrhous stomach cancer. Cancer Sci 96: 323–332.
17. Yanagihara K, Tanaka H, Takigahira M, Ino Y, Yamaguchi Y, et al. (2004) Establishment of two cell lines from human gastric scirrhous carcinoma that possess the potential to metastasize spontaneously in nude mice. Cancer Sci 95: 575–582.
18. Miyazawa Y, Uekita T, Hiraoka N, Fujii S, Kosuge T, et al. (2010) CUB domain-containing protein 1, a prognostic factor for human pancreatic cancers, promotes cell migration and extracellular matrix degradation. Cancer Res 70: 5136–5146.
19. Yamaguchi H, Yoshida S, Muroi E, Yoshida N, Kawamura M, et al. (2011) Phosphoinositide 3-kinase signaling pathway mediated by p110{alpha} regulates invadopodia formation. J Cell Biol 193: 1275–1288.
20. Sanz-Moreno V, Gaggioli C, Yeo M, Albrengues J, Wallberg F, et al. (2011) ROCK and JAK1 signaling cooperate to control actomyosin contractility in tumor cells and stroma. Cancer Cell 20: 229–245.
21. Vicente-Manzanares M, Ma X, Adelstein RS, Horwitz AR (2009) Non-muscle myosin II takes centre stage in cell adhesion and migration. Nat Rev Mol Cell Biol 10: 778–790.
22. Narumiya S, Tanji M, Ishizaki T (2009) Rho signaling, ROCK and mDia1, in transformation, metastasis and invasion. Cancer Metastasis Rev 28: 65–76.
23. Schenone S, Brullo C, Musumeci F, Botta M (2010) Novel dual Src/Abl inhibitors for hematologic and solid malignancies. Expert Opin Investig Drugs 19: 931–945.
24. Butcher DT, Alliston T, Weaver VM (2009) A tense situation: forcing tumour progression. Nat Rev Cancer 9: 108–122.
25. Parekh A, Weaver AM (2009) Regulation of cancer invasiveness by the physical extracellular matrix environment. Cell Adh Migr 3: 288–292.
26. Ura H, Obara T, Yokota K, Shibata Y, Okamura K, et al. (1991) Effects of transforming growth factor-beta released from gastric carcinoma cells on the contraction of collagen-matrix gels containing fibroblasts. Cancer Res 51: 3550–3554.
27. Nakazawa K, Yashiro M, Hirakawa K (2003) Keratinocyte growth factor produced by gastric fibroblasts specifically stimulates proliferation of cancer cells from scirrhous gastric carcinoma. Cancer Res 63: 8848–8852.
28. Tendo M, Yashiro M, Nakazawa K, Yamada N, Hirakawa K (2005) Inhibitory effect of a selective cyclooxygenase inhibitor on the invasion-stimulating activity of orthotopic fibroblasts for scirrhous gastric cancer cells. Cancer Sci 96: 451–455.
29. Yashiro M, Chung YS, Kubo T, Hato F, Sowa M (1996) Differential responses of scirrhous and well-differentiated gastric cancer cells to orthotopic fibroblasts. Br J Cancer 74: 1096–1103.
30. Yashiro M, Nakazawa K, Tendo M, Kosaka K, Shinto O, et al. (2007) Selective cyclooxygenase-2 inhibitor downregulates the paracrine epithelial-mesenchymal interactions of growth in scirrhous gastric carcinoma. Int J Cancer 120: 686–693.
31. Calvo F, Ege N, Grande-Garcia A, Hooper S, Jenkins RP, et al. (2013) Mechanotransduction and YAP-dependent matrix remodelling is required for the generation and maintenance of cancer-associated fibroblasts. Nat Cell Biol 15: 637–646.

Acknowledgments

We thank Emi Saito for technical assistance. We are grateful to Screening Committee of Anticancer Drugs supported by Grant-in-Aid for Scientific Research on Innovative Areas, Scientific Support Programs for Cancer Research, from the Ministry of Education, Culture, Sports, Science and Technology of Japan.

Author Contributions

Conceived and designed the experiments: HY RS. Performed the experiments: HY NY MT YI. Contributed reagents/materials/analysis tools: KF KY MY. Wrote the paper: HY RS.

Published OnlineFirst February 25, 2013; DOI: 10.1158/1541-7786.MCR-12-0544

Molecular Cancer Research

Oncogenes and Tumor Suppressors

CDCP1 Regulates the Function of MT1-MMP and Invadopodia-Mediated Invasion of Cancer Cells

Yuri Miyazawa[1], Takamasa Uekita[1], Yuumi Ito[1,2], Motoharu Seiki[3], Hideki Yamaguchi[1], and Ryuichi Sakai[1]

Abstract

Complement C1r/C1s, Uegf, Bmp1 (CUB) domain-containing protein 1 (CDCP1) is a transmembrane protein that regulates anchorage-independent growth and cancer cell migration and invasion. Expression of CDCP1 is detected in a number of cancer cell lines and tissues and is closely correlated with poor prognosis. Invadopodia are actin-based protrusions on the surface of invasive cancer cells that promote the degradation of the extracellular matrix (ECM) via localized proteolysis, which is mainly mediated by membrane type 1 matrix metalloproteinase (MT1-MMP). MT1-MMP is accumulated at invadopodia by targeted delivery via membrane trafficking. The present study shows that CDCP1 is required for ECM degradation by invadopodia in human breast cancer and melanoma cells. CDCP1 localized to caveolin-1–containing vesicular structures and lipid rafts and was detected in close proximity to invadopodia. Further biochemical analysis revealed that substantial amounts of CDCP1 existed in the Triton X-100 insoluble lipid raft fraction. CDCP1 was coimmunoprecipitated with MT1-MMP and colocalized with MT1-MMP at the vesicular structures. The siRNA-mediated knockdown of the CDCP1 expression markedly inhibited MT1-MMP–dependent ECM degradation and Matrigel invasion and reduced the accumulation of MT1-MMP at invadopodia, as shown by immunofluorescence analysis. These results indicate that CDCP1 is an essential regulator of the trafficking and function of MT1-MMP- and invadopodia-mediated invasion of cancer cells. *Mol Cancer Res; 11(6); 628–37.* ©*2013 AACR.*

Introduction

Complement C1r/C1s, Uegf, Bmp1 (CUB) domain-containing protein 1 (CDCP1), also described as SIMA135 and TRASK (1, 2), is a type 1 transmembrane protein with 3 CUB domains as the extracellular domains and several tyrosine residues that can be phosphorylated by Src family kinases (SFK) in the intracellular domain (1–6). The expression of CDCP1 was reported in several human malignancies, such as colon and breast cancers (3, 7). CDCP1 expression is strongly associated with cancer progression and poor prognosis in renal cell carcinoma, lung adenocarcinoma, and pancreatic cancer (8–10). We previously reported that CDCP1 is a critical regulator of anoikis resistance in lung cancer cells (11), peritoneal dissemination of gastric scirrhous carcinoma (12), and invasion of pancreatic cancer cells (8). We showed that knockdown of CDCP1 resulted in the inhibition of extracellular matrix (ECM) degradation by pancreatic cancer cells (8). Tyrosine phosphorylation of CDCP1, especially at tyrosine 734 residue, plays an essential role in these oncogenic processes (8, 11, 12). However, the exact molecular mechanisms by which CDCP1 regulates cancer cell invasion remain to be determined.

Matrix metalloproteinases (MMP) have been implicated in many aspects of cancer progression, such as tumor growth, angiogenesis, invasion, and metastasis (13). Among MMPs, membrane type 1 (MT1)-MMP, the first discovered membrane-type MMP (14), plays a pivotal role in ECM degradation at the leading edge of invasive cancer cells (15). Clinically, MT1-MMP expression is strongly associated with cancer progression and metastasis (16) and poor prognosis of patients (17, 18). A cell–surface complex consisting of MT1-MMP oligomers binds to inactive proMMP-2 and mediates its cleavage and activation (19). In addition to activating secreted MMPs, MT1-MMP plays a key role in cancer invasion through its interaction and processing of cell surface proteins including CD44 (20). MT1-MMP function can be regulated by clathrin-mediated or caveolar endocytosis followed by degradation in the lysosomal compartment (21).

Invadopodia are unique protrusions observed at the cell adhesion sites of invasive cancer cells that are rich in cell-ECM adhesion molecules, actin assembly regulators, membrane-remodeling proteins, tyrosine kinases, tyrosine-phosphorylated proteins, and MMPs (22, 23). Because they offer an environment that supports ECM

Authors' Affiliations: [1]Division of Metastasis and Invasion Signaling, National Cancer Center Research Institute; [2]Laboratry of Genome and Biosignal, Tokyo University of Pharmacy and Life Sciences; and [3]Division of Cancer Cell Research, Institute of Medical Science, The University of Tokyo, Tokyo, Japan

Corresponding Author: Ryuichi Sakai, National Cancer Center Research Institute, 5-1-1 Tsukiji, Chuo-ku, Tokyo 104-0045, Japan. Phone: 81-3-3547-5247; Fax: 81-3-3542-8170; E-mail: rsakai@ncc.go.jp

doi: 10.1158/1541-7786.MCR-12-0544

Published OnlineFirst February 25, 2013; DOI: 10.1158/1541-7786.MCR-12-0544

degradation and thus cancer invasion and metastasis, the ability to form invadopodia is closely associated with the invasive and metastatic potentials of cancer cells (24, 25). The matrix degradation activity at invadopodia is dependent on the accumulation and activation of MT1-MMP at the cell surface of invadopodia (26–28). Recent studies have revealed that endocytic and exocytic trafficking are critical for the targeted delivery of MT1-MMP to invadopodia (21, 29–31). However, the molecular mechanisms that control the delivery and function of MT1-MMP at invadopodia are not fully understood. In this study, we show that CDCP1 regulates the function of MT1-MMP and plays an essential role in ECM degradation at invadopodia in human cancer cells.

Materials and Methods

Cell culture and transfection

The human breast cancer cell line MDA-MB-231 and the human melanoma cell line RPMI 7951 were obtained from the American Type Culture Collection. MDA-MB-231 and RPMI 7951 cells were maintained in a 1:1 mixture of high-glucose Dulbecco's modified Eagle's medium and RPMI-1640 supplemented with 10% FBS, 10 U/mL penicillin, and 10 μg/mL streptomycin. The cells were transfected with the indicated plasmids, using Lipofectamine 2000 or Lipofectamine LTX (Life Technologies Corporation) according to the manufacturer's instructions.

siRNA treatment

Two sets of siRNA against CDCP1 were synthesized and purchased from Life Technologies Corporation as described elsewhere (12). The control siRNA for CDCP1 was synthesized as follows: CDCP1 control siRNA-1, 5′-GCUACCGGAGCGAAACAACAUCUUA-3′ (sense), and 5′-UAAGAUGUUGUUUCGCUCCGGUAGC-3′ (antisense). siRNAs (40 pmol) were incorporated into cells using Lipofectamine 2000 or Oligofectamine (Life Technologies Corporation), according to the manufacturer's instructions. The cells were subjected to further experiments 72 hours after the siRNA treatment.

Plasmids, antibodies, and reagents

To generate the GFP-MT1-MMP construct, human MT1-MMP cDNA was subcloned into the pEGFP-N1 vector (Clontech Laboratories Inc.; ref. 29). Human MT1-MMP having a FLAG-tag at the N-terminus (MT1-F) was subcloned into the pSG5 vector (Sigma; ref. 32). The polyclonal antibodies against CDCP1 and tyrosine-phosphorylated CDCP1 (Tyr734) were prepared as described previously (8). The anti-MT1-MMP antibody (1D8) was prepared as described previously (33). Other antibodies used were α-tubulin (B-5-1-2; Sigma), cortactin (4F11; Millipore), caveolin-1 (610493; BD Biosciences), early endosome antigen 1 [EEA-1 (610457; BD Biosciences)], MT1-MMP (ab38971; Abcam), GFP (ab1218, Abcam; 04363-24, Nacalai Tesque), CDCP1 (ab1377; Abcam), Syntaxin 6 (C34B2; Cell Signaling Technology Inc.), and Tks5 (sc-9945; Santa Cruz Biotechnology).

Western blotting and immunoprecipitation

The Western blotting and immunoprecipitation were conducted as described previously (8). The cells were lysed with a buffer (20 mmol/L Tris-HCl, at pH 7.4, 150 mmol/L NaCl, 1 mmol/L EDTA, 20 mmol/L NaF, 1% Nonidet P-40, 5% glycerol, and 2% octyl-β-D-glucoside plus protease inhibitor) for dissolution of lipid rafts and subjected to Western blotting and immunoprecipitation. Protein concentration was determined using the Bicinchoninic Acid Protein Assay Kit (Thermo Fisher Scientific Inc.), and equal amounts of protein were separated by SDS-PAGE. A polyvinylidene difluoride membrane (Immobilon-P, Millipore) was used as the transfer membrane, and Blocking One (Nacalai Tesque) was used for blocking the membrane. For immunoprecipitation, 1 mg of protein was mixed with 5 μg of CDCP1 antibody and rotated with Protein G Sepharose beads (GE Healthcare) or 10 μL FLAG M2 agarose beads (Sigma).

Invadopodia assay

Fluorescent gelatin-coated coverslips were prepared as described previously (29, 34). MDA-MB-231 and RPMI 7951 cells were cultured for 3 to 7 hours on coverslips coated with fluorescent gelatin. In the case of the cells overexpressing MT1-MMP, they were cultured on the gelatin matrix for 2 hours. To quantitate the degradation activity of invadopodia, 20 randomly selected fields, usually containing 20 to 40 cells, were imaged with a × 60 objective for each determination. The degradation area was determined by using the ImageJ software version 1.41o and normalized for the number of cells. In each analysis, the mean value of the control cells was set at 100%, and the relative values of the cells treated with siRNAs were then calculated. The relative number of invadopodia per cell was determined by counting punctate F-actin structures that were positive for Tks5. The mean (SE) of at least 3 independent determinations was calculated.

Invasion assay

The invasion assay was conducted using modified Transwell chambers with a polycarbonate nucleopore membrane (BD Falcon), as described previously (8). The top side of the membrane was coated with 0.02% collagen (Cellmatrix Type I-A, Nitta Gelatin Inc.). The cells treated with each siRNA were seeded onto the top part of each chamber. After incubation for 30 hours, the cells on the membrane were fixed. The number of migrated or invaded cells was determined by counting the cells on the bottom side of the membranes from 2 wells (2 fields per membrane) at a magnification of × 100, and the extent of invasion was expressed as the average ratio (number of cells transfected with siRNA per field/average number of cells transfected with control siRNA per field). The results were expressed as the mean of 3 independent experiments.

Immunofluorescence

Immunofluorescence was conducted as previously described (34). Briefly, the cells were fixed in 4%

Published OnlineFirst February 25, 2013; DOI: 10.1158/1541-7786.MCR-12-0544

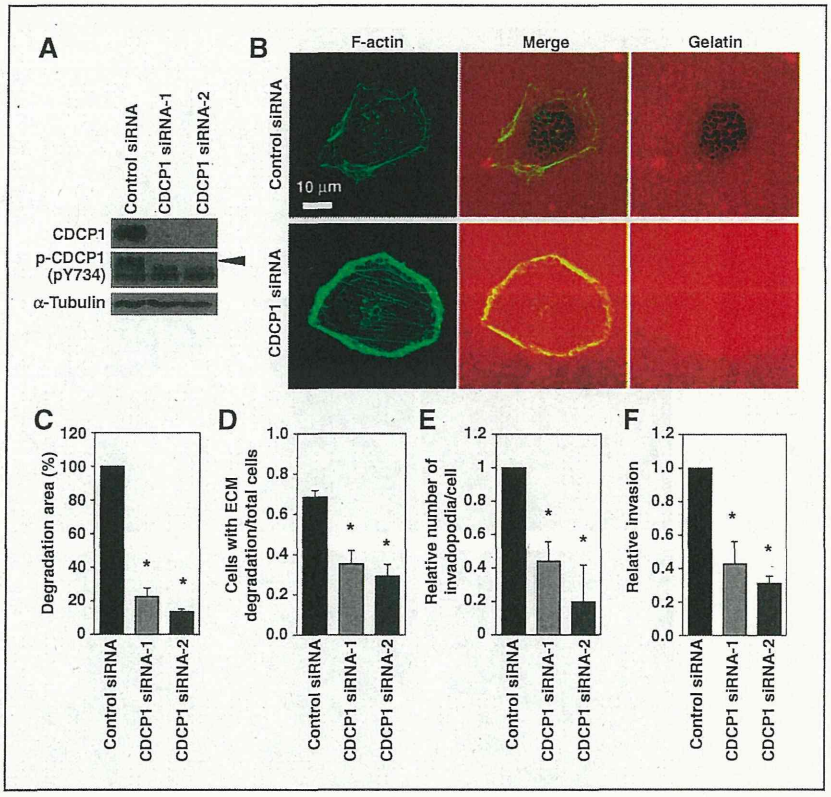

Figure 1. CDCP1 is required for invadopodia formation and ECM degradation by human breast cancer cells. A, the MDA-MB-231 cells were treated with control or CDCP1 siRNAs and subjected to Western blotting with the indicated antibodies. The black arrowhead shows CDCP1. B, the cells treated with the indicated siRNAs were cultured on fluorescent gelatin-coated coverslips for 7 hours and stained for F-actin. C, the areas showing degradation of the fluorescent gelatin matrix were quantified as described in the Materials and Methods. D, the proportion of the cells showing degradation of the gelatin matrix. E, the relative number of invadopodia per cell. F, the result of the invasion assay of the MDA-MB-231 cells treated with CDCP1 siRNAs. Columns, mean; bars, SD. *, $P < 0.05$.

paraformaldehyde for 15 minutes and permeabilized with 0.1% Triton X-100 for 5 minutes. The cells were blocked in 1% bovine serum albumin and 1% goat serum for 30 minutes, incubated with primary antibodies for 1 hour, and then incubated with Alexa Fluor-conjugated secondary antibodies and phalloidin (Life Technologies Corporation) for 30 minutes. The samples were observed with an IX81-ZDC-DSU confocal microscope (Olympus) equipped with a cooled CCD camera (ORCA-ER, Hamamatsu Photonics), and the imaging system was driven by the MetaMorph software (Universal Imaging). All the images were acquired using × 60 (PLAPON60XO, NA 1.42) or × 100 oil objectives (UPLSAPO100XO, NA 1.4). The images were analyzed and processed with various software packages, including MetaMorph, ImageJ version 1.41o (NIH, Bethesda, MD; http://rsbweb.nih.gov/ij/), and Adobe Photoshop CS4. The relative distribution of CDCP1 at the cell periphery versus intracellular vesicles was determined by calculating the ratio between the fluorescence intensities of peripheral and perinuclear vesicular CDCP1 from confocal images. For colocalization analysis, Mander overlap coefficient was calculated using ImageJ with Just Another Colocalization Plugin. All calculations were conducted on 8 to 20 cells.

Labeling cells with CTxB

The cells cultured on gelatin-coated coverslips were washed with ice-cold PBS and incubated with 10 μg/mL Alexa Fluor-conjugated cholera toxin B subunit (CTxB; Life Technologies Corporation) in PBS for 20 minutes on ice. For the internalization experiments, the cells were labeled with CTxB in the growth medium for 20 minutes on ice and then incubated for the indicated times at 37°C. The cells were stained with anti-CDCP1 antibody as described previously.

Cell fractionation

Cell fractionation was conducted as described previously (29). The cytosolic fraction was extracted with the

Published OnlineFirst February 25, 2013; DOI: 10.1158/1541-7786.MCR-12-0544

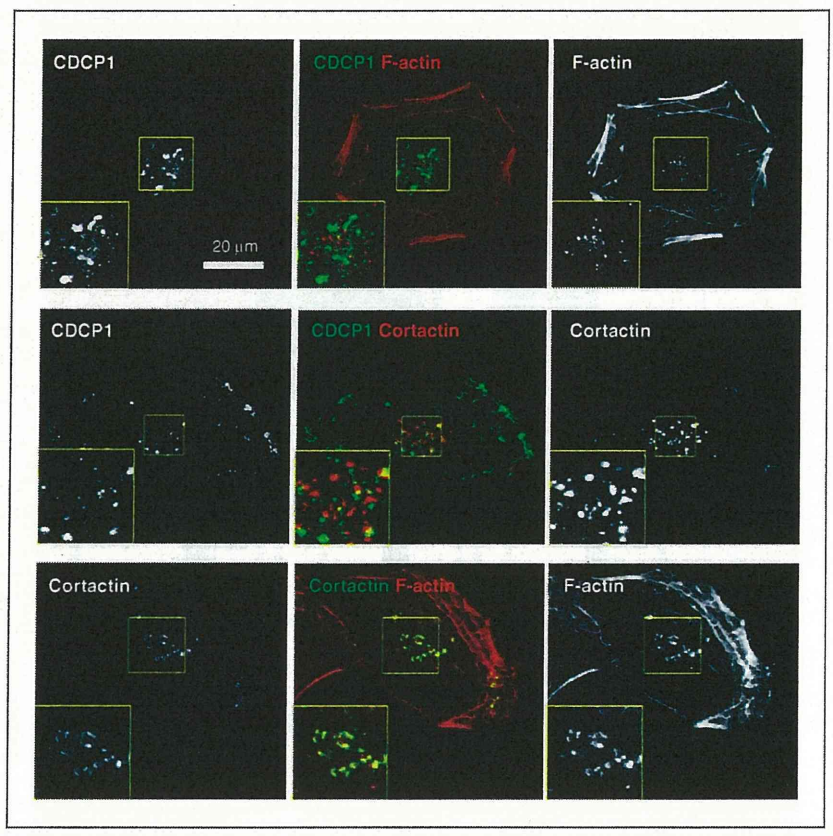

Figure 2. Localization of CDCP1 at invadopodia. The MDA-MB-231 cells were cultured on gelatin-coated coverslips and stained for CDCP1, cortactin, and F-actin. Top, F-actin (red) and CDCP1 (green); middle, cortactin (red) and CDCP1 (green); bottom, F-actin (red) and cortactin (green). The inserts are the magnified images of the boxed regions.

ProteoExtract Subcellular Proteome Extraction Kit (Millipore). Triton X-100 soluble materials were then extracted with a buffer (25 mmol/L Tris-HCl at pH 7.5, 150 mmol/L NaCl, 5 mmol/L EDTA, and protease inhibitors) containing 1% Triton X-100. Insoluble materials were further extracted with TNE buffer containing 1% SDS. Equal amounts of protein from each fraction were analyzed by immunoblotting.

Results

CDCP1 regulates invadopodia-mediated ECM degradation

The expression of CDCP1 in various cancers, including breast cancer, has been reported previously (7). We examined several human breast cancer cell lines and detected significant CDCP1 expression in MDA-MB-453, BT549, and MDA-MB-231 cells, using Western blotting (Supplementary Fig. S1). The immunoblotting with a phospho-specific antibody against Y734 of CDCP1 revealed tyrosine phosphorylation of CDCP1 in the highly invasive cell line BT549 and MDA-MB-231 (Fig. 1A and Supplementary Fig. S1), suggesting that CDCP1-mediated signaling might play a role in breast cancer cell invasion. Because invadopodia formation in MDA-MB-231 cells has been reported previously (35), we used this cell line to investigate the potential role of CDCP1 in invadopodia formation and function.

MDA-MB-231 cells were treated with 2 independent siRNAs against CDCP1 and subjected to Western blotting, which showed that CDCP1 expression was successfully suppressed by both siRNAs (Fig. 1A). The siRNA-treated cells were cultured on coverslips coated with fluorescent gelatin and tested for invadopodia formation and gelatin degradation. Gelatin degradation, which was primarily localized to the area around the invadopodia in MDA-MB-231 cells, was significantly decreased by treatment with CDCP1 siRNA, as shown by immunofluorescence and quantitative analysis of the degradation area (Fig. 1B and C). In addition, the proportion of cells with apparent degradation of the gelatin matrix was clearly decreased by CDCP1 knockdown (Fig. 1D). We also observed that CDCP1 knockdown significantly suppressed degradation of gelatin matrix by RPMI 7951 human melanoma cells (Supplementary Fig. S2A and S2B). It is known that assembly of actin-core structures and subsequent focal concentration of MMPs are both required for ECM degradation by invadopodia. The number of invadopodia that were punctate F-actin structures positive for an invadopodia marker Tks5 per cell was significantly decreased in cells transfected with CDCP1 siRNA (Fig. 1E). These observations indicate that CDCP1

Published OnlineFirst February 25, 2013; DOI: 10.1158/1541-7786.MCR-12-0544

is required for both assembly of invadopodia structures and ECM degradation activity. In addition, reduced expression of CDCP1 significantly suppressed invasion of MDA-MB-231 cells through Matrigel (Fig. 1F), which is consistent with our results obtained with gastric and pancreatic cancer cell lines (8, 12). Taken together, these results indicate that CDCP1 is an essential regulator of invadopodia-mediated ECM degradation during cancer cell invasion.

CDCP1 localizes to lipid raft-containing vesicular structures associated with invadopodia

To determine the cellular localization of CDCP1 in MDA-MB-231 cells, we conducted immunocytostaining with a specific antibody against CDCP1. Distinct signals for CDCP1 were observed as punctate and vesicular structures within the cells, and the signals were also detected at the cell periphery (Fig. 2). Quantitative analysis of fluorescence intensities showed that the ratio between perinuclear vesicular and peripheral CDCP1 was 0.42 ± 0.12 (SD, $N = 23$). These CDCP1 signals did not colocalize with invadopodia, which were observed as punctate structures at the cell-matrix adherent site showing positive staining for the invadopodia markers F-actin and cortactin. Nevertheless, strong vesicular CDCP1 signals were consistently observed in close proximity to invadopodia.

To identify the vesicular structures containing CDCP1, we conducted immunofluorescence analysis with several organelle markers. Syntaxin 6 is a *trans*-Golgi network protein and regulates membrane trafficking (36). Partial colocalization of CDCP1-containing vesicles with syntaxin

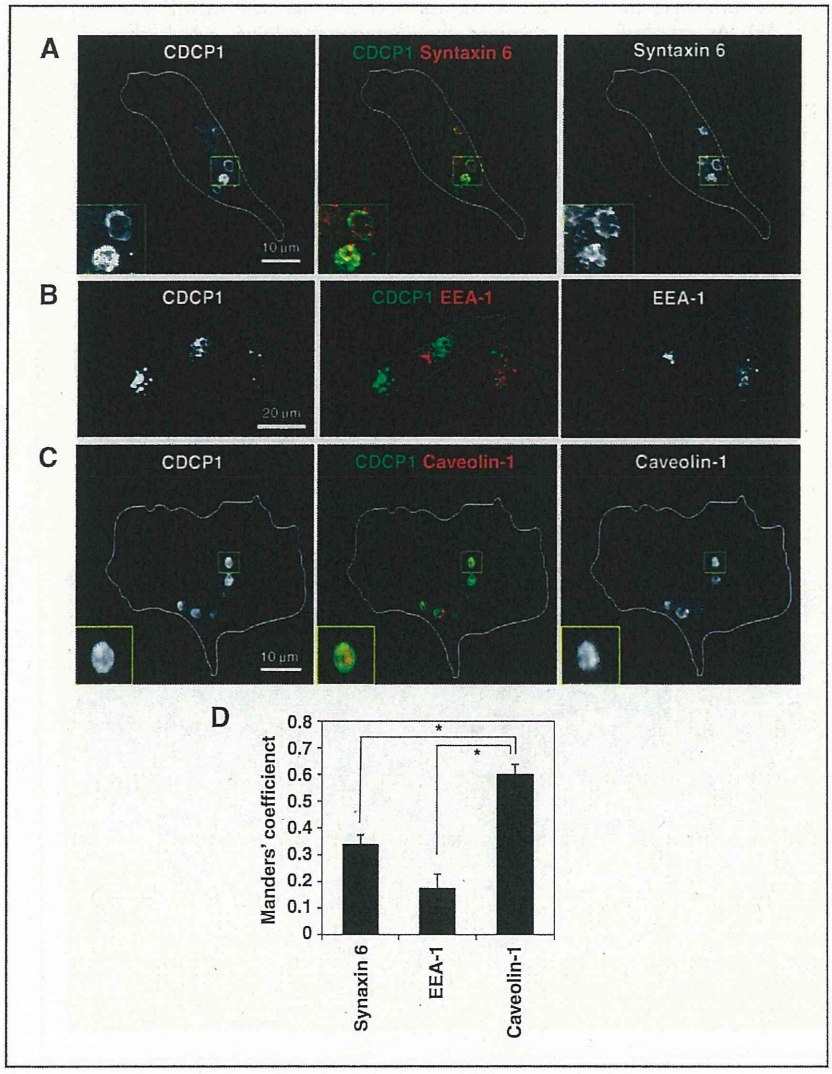

Figure 3. CDCP1 localizes to intracellular vesicles containing caveolin-1. The MDA-MB-231 cells were cultured on gelatin-coated coverslips and costained for CDCP1 with syntaxin 6 (A), EEA-1 (B), and caveolin-1 (C). Inserts are magnified images of the boxed regions. D, Mander coefficient was calculated on the basis of the degree of colocalization between CDCP1 and each vesicular marker from confocal immunofluorescence micrographs. Columns, mean; bars, SE. *, $P < 0.00001$.

Published OnlineFirst February 25, 2013; DOI: 10.1158/1541-7786.MCR-12-0544

6 (Fig. 3A) indicated that CDCP1 proteins are delivered through and/or function in the *trans*-Golgi network. CDCP1 did not colocalize with EEA-1, an early endosome marker (Fig. 3B), whereas it markedly colocalized with caveolin-1 in vesicular structures (Fig. 3C). Quantitative analysis of confocal images confirmed these observations and showed significant colocalization of CDCP1 with caveolin-1 (Fig. 3D).

Caveolin-1, an essential component of a subtype of lipid rafts called caveolae, regulates the organization and dynamics of lipid rafts and plays a role in membrane trafficking by regulating caveola/raft-dependent endocytosis (37). To determine whether CDCP1 is present in lipid rafts, MDA-MB-231 cells cultured on gelatin-coated dishes were separated into cytosolic, Triton X-100–soluble, and Triton X-100–insoluble fractions, and analyzed by Western blotting (Fig. 4A). Lipid rafts are known to be enriched in the Triton X-100–insoluble fraction (38, 39). As expected, CDCP1 was hardly detected in the cytosolic fraction but was concentrated in the Triton X-100–soluble membrane fraction. It is important to note that a significant amount of CDCP1 was also detected in the Triton X-100–insoluble fraction (Fig. 4A), indicating that CDCP1 exists in lipid rafts. Cells were then labeled with fluorescent CTxB, a lipid raft marker (40), and the course of CTxB internalization and localization of CDCP1 was simultaneously followed by immunofluorescence (Fig. 4B). Before the internalization, CTxB signals partly colocalized with CDCP1 at the ventral surface of the cell. The internalization of CTxB caused a shift of CTxB fluorescence to intracellular endosomes, where it colocalized with CDCP1 signals, starting 10 minutes after internalization and lasting until at least 60 minutes (Fig. 4B). Quantitative analysis of colocalization of CDCP1 and CTxB confirmed these observations (Fig. 4C). These results indicate that CDCP1 mainly exists in vesicular compartments where internalized lipid raft membranes accumulate.

CDCP1 colocalizes and associates with MT1-MMP

We previously reported that caveolin-1 colocalizes with MT1-MMP at lipid raft-enriched vesicles and regulates ECM degradation by invadopodia (29). The possible interaction between CDCP1 and MT1-MMP was therefore examined by immunocytostaining, which showed that MT1-MMP colocalized with CDCP1 at the vesicular structures (Fig. 5A). Mander coefficient for the degree of CDCP1 signals colocalizing with MT1-MMP was 0.63 ± 0.039 (SE, $N = 17$), which was very similar to that for CDCP1 colocalizing with caveolin-1 (Fig. 3D). In addition, the coimmunoprecipitation analysis conducted using MDA-MB-231 cells treated with octyl glucoside, which solubilizes

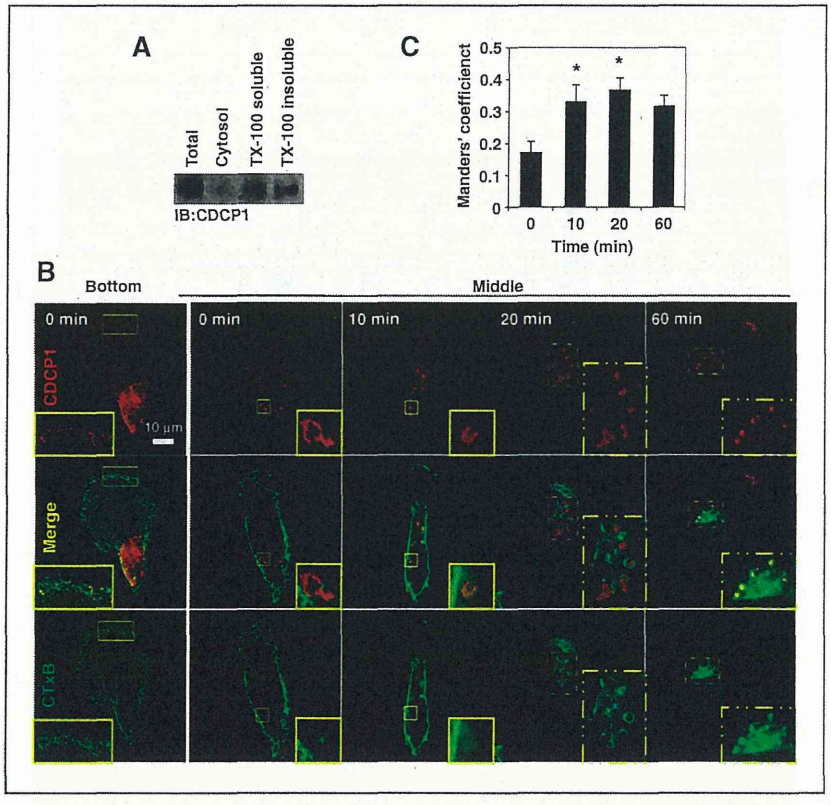

Figure 4. CDCP1 localizes to intracellular vesicles containing lipid rafts. A, the MDA-MB-231 cells were directly lysed or separated into cytosolic and Triton X-100–soluble and Triton X-100–insoluble fractions. The presence of CDCP1 in each fraction was determined by immunoblotting. B, the MDA-MB-231 cells cultured on gelatin-coated coverslips were labeled with fluorescent CTxB on ice and incubated at 37°C for the indicated time to allow internalization of CTxB. The cells were then stained with an anti-CDCP1 antibody. Before internalization (0 minute), CDCP1 was mainly detected in the intracellular vesicles (middle) and partly at the cell periphery, where it colocalized with CTxB (bottom). As internalization proceeded (10–60 minutes), CTxB signals were detected in the intracellular vesicles colocalized with CDCP1. The inserts are magnified images of the boxed regions. C, Mander coefficient was calculated to determine the degree of colocalization between CDCP1 and CTxB at different time points. Columns, mean; bars, SE. *, $P < 0.01$.